7th International Conference on Debris-Flow Hazards Mitigation

Regional-scale modelling of liquefaction-induced shallow landslides in unsaturated slopes

Xiang Li[a], Zhichen Song[b], José J. Lizárraga[a*], Giuseppe Buscarnera[a]

[a]*Northwestern University, 633 Clark Street, Evanston 60208, USA*
[b]*Central South University, Shaoshan South RD, Changsha 410075, China*

Abstract

Regional modelling of rainfall-induced landslide triggering poses several technical challenges. These events can originate from a number of hydro-mechanical processes, such as soil-strength degradation, development of localized zones of pore-water pressures, liquefaction, among others. At the same time, the interplay between the spatial variability of topographic attributes, soil properties and transient infiltration can lead to a widespread distribution of distinct slope failure mechanisms across the same landscape. To this aim, this contribution describes a simulation platform for the efficient generation of storm-induced, landslide susceptibility maps in which different slope instability mechanisms can be considered. The framework relies on a vectorized finite element (FE) algorithm that performs fully-coupled simulations of transient infiltration in unsaturated soils, while input and output processing stages are linked to a Geographical Information System. To illustrate the capabilities of the proposed framework, the role of several hydro-mechanical processes on the inception of slope instability are first explored (i.e., coupled flow-deformation analyses, constitutive couplings). After this, results of regional-scale simulations are presented, where it is shown that such considerations can affect the computed spatio-temporal patterns of landslide triggering. Lastly, approaches to incorporate uncertainty of input data into landslide susceptibility zonation by using spatially-correlated random fields are discussed. The proposed framework provides an important step towards the development of robust, physically-based models for regional landslide hazard assessment.

Keywords: flowslides; shallow landslides; infiltration; distributed modelling; spatial uncertainty

1. Introduction

During the last decades, analyses of landslide hazard zonation on urban areas have gained considerable attention (Guzzetti et al., 1999). Indeed, the advent of Geographical Information Systems (GIS), advances in computational resources and remote-sensing technologies have opened new avenues for the development of data-driven, physically-based models of regional landslide forecasting. Such models aim to infer and analyze the factors responsible for slope instabilities across a geological setting by combining principles of hydrology and mechanics (Montgomery and Dietrich, 1994; Baum et al., 2010; Milledge et al., 2014). Among their key challenges is the ability to incorporate advanced features of soil-moisture interactions (i.e. coupled flow soil-deformation processes, inelastic soil response, layered profiles) and uncertainty quantification into a unified framework.

This contribution presents a versatile computational platform for regional analyses of shallow-landslide susceptibility. To provide description of its functionality, a well-documented series of rainfall-induced landslides in volcanic soils is used as a background case study. The paper is structured in three parts, namely, i) a presentation of the model equations; ii) examples of regional-scale landslide triggering zonation; iii) modelling spatial uncertainty of input properties. Details of specific implementation procedures are shown in other references. Here, the aim is to provide an overall description of the current model capabilities and discuss future areas of improvement.

* Corresponding author e-mail address*: jjlizarraga@u.northwestern.edu*

2. Governing equations

2.1. Field equations

The discussion is focused on shallow unsaturated sloping ground. For an infinite slope, in the absence of variations of body forces, the balance of linear momentum for an incremental loading process is given by:

$$\frac{\partial \dot{\sigma}}{\partial z} = 0, \qquad \frac{\partial \dot{\tau}}{\partial z} = 0 \tag{1}$$

where σ and τ represent the total normal and shear stresses, respectively, z is the coordinate in the direction normal to the slope and the upper dot denotes rate terms. Balance of water mass in the presence of constant air pressure leads to:

$$S_r \dot{\varepsilon} + n \frac{\partial S_r}{\partial h} \dot{h} - \frac{\partial}{\partial z}\left(K \frac{\partial h}{\partial z} \right) - \frac{\partial K}{\partial z} \cos\alpha = 0 \tag{2}$$

where S_r is the degree of saturation, ε is the normal strain, n is the porosity, h is the pressure head (negative values representing suction), K is the hydraulic conductivity, and α is the slope angle. The mechanical behaviour of the soil skeleton is here hypothesized to be governed by the effective stress σ':

$$\sigma = \sigma' + \chi_k \left(\gamma_w h \right) \tag{3}$$

where γ_w is the unit weight of water, and χ_k is an effective stress parameter. A constitutive relationship of the soil skeleton is required to complete the problem formulation. While general inelastic constitutive laws written in incremental form can be used, linear elasticity is used here for illustrative purposes i.e., $\dot{\sigma}' = E\dot{\varepsilon}, \ \dot{\tau} = G\dot{\gamma}$ where E and G are material constants. Additionally, constitutive relationships for the hydraulic variables are required i.e., $S_r = F_w\left(s\right), \ K = F_k\left(s\right)$ where $s = \gamma_w h$ is the matric suction, while F_w and F_k are functions known as the *Water Retention Curve* (WRC) and *Hydraulic Conductivity Function* (HCF), respectively. Substituting them into (1) and (2) and imposing appropriate initial and boundary conditions completes the initial boundary-value problem (IBVP) to solve.

3. Analyses of single slopes

3.1. Effects of soil deformability on infiltration analyses

The solution of the coupled system of PDE is solved numerically. Specifically, a Galerkin Finite Element discretization and an explicit forward numerical scheme are used (Sheng et al., 2003). To illustrate the hydro-mechanical feedbacks occurring during the infiltration process, examples of simulations will be shown in the following. A schematic representation of the model initial and boundary conditions for the case of an infiltration problem is shown in Fig. 1.

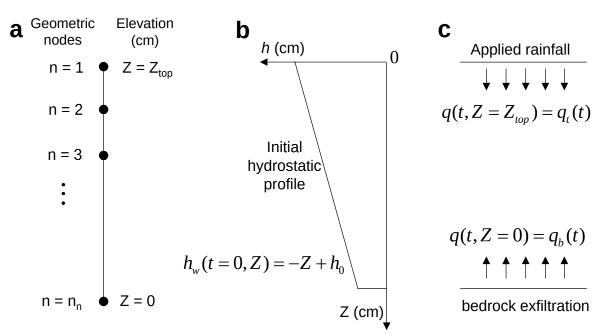

Fig. 1. Schematic representation the infiltration problem: (a) mesh structure and problem domain, (b) initial profile, and (c) boundary conditions.

Consider first the case of constant rainfall rate $q = K$, in which the role of soil deformations is neglected (i.e., rigid soil skeleton). The computed profiles of h are shown in Fig. 2a with continuous lines, while time histories at two different locations are shown in Fig. 2b. As expected, the pressure head increases during the infiltration process, such that at a depth of z = 4m an increment of Δh = 2m is computed after 30 hrs.

To analyze the role of soil deformability, a linear elastic model is used to characterize the mechanical behavior of the soil. In this case, the reduction of pressure head driven by the infiltration process causes a decrease of the effective stress, hence promoting swelling and lower values of h when compared against the rigid case. In other words, soils that expand upon wetting hinder the development of high pore pressures during infiltration. Alternatively, soils that compact upon infiltration are detrimental for slope stability, in that they can cause elevated values of h. The role of such effects can be modeled by introducing an additional elastic modulus that controls the amount of compaction upon changes of suction (Wu et al., 2016). This illustrated in Fig 2, where an increment of Δh = 2.5 m at z = 4 m is computed after 30 hrs. Such examples highlight the importance of modelling the role of coupled hydro-mechanical processes into slope stability analyses.

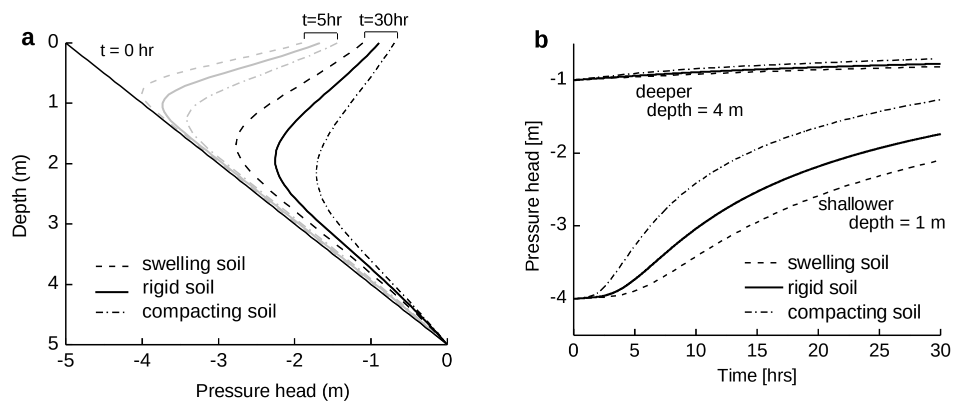

Fig. 2. Comparison of model simulations using different soil deformability properties: (a) profiles and (b) time histories of pressure head.

3.2. Modelling flowslide susceptibility

Debris flows can be the outcome of different mechanisms. For instance, they can originate from marginally stable slopes that start to move when driving forces overcome their soil frictional resistance. As they propagate downslope, they can grow in size by entraining sediments and water (Iverson, 2014).

The inception of soil failure due sharp fluid pressurization can also promote the spontaneous acceleration of soil masses (a phenomenon known as soil liquefaction) even before the entrainment of sediments (Dawson et al., 1998). Indeed, full or partial liquefaction in granular soils is among the key factors responsible for highly mobile landslides, which are referred as flowslides when liquefaction takes place directly at the source (Hungr et al., 2001). Such definition is adopted in this work.

Soil liquefaction is an unstable process that is highly dependent on the hydro-mechanical properties of the material. For example, it is well known that soils that dilate upon shearing are less prone to liquefaction than those that contract (Jefferies and Been, 2015). Similarly, materials that compact upon wetting, such as residual soils, loess and volcanic materials, also display susceptibility to liquefy due to their high capability to retain pore water and their loose internal packing (Picarelli et al., 2008). Thus, defining landslide triggering thresholds that explicitly incorporate such features of soil behavior into slope stability analyses can be useful for enhanced landslide hazard modeling platforms.

A possible approach was proposed by Lizárraga and Buscarnera, 2017. In summary, failure thresholds were derived by analyzing the soil response within an unsaturated shallow slope under two scenarios: uncoupled *drained* response (where failure conditions are referred to as slips) and coupled failures driven by the pressurization of pore water and soil plastic response (referred to as flowslides). A simple rigid-plastic constitutive law was used. Particularly, the response of the soil was modelled with a non-associated flow rule based on logarithmic expressions of yield function and plastic potential, as well as through an exponential hardening law dependent on plastic strains and suction. In this way, conditions that reflect instability (i.e., a mathematical singularity of the equations) were expressed explicitly in terms of soil properties, eventually casting them into the following safety factors (FS):

$$FS_{SLIPS} = \frac{\tan\alpha}{\tan\phi'}\left(1+\frac{\chi_k s}{\sigma}\right), \quad FS_{FLOWS} = \frac{\tan\alpha}{\tan\phi^{LIQ}}\left(1+\frac{\chi_k s}{\sigma}\right)\chi_w \tag{4}$$

At zero suction, FS_{SLIPS} converges to the classical definition of FS for saturated infinite slopes. The coefficient χ_w is a function of the deformation/wetting properties of the unsaturated soil (Lizárraga and Buscarnera, 2017). Depending on the prevailing hydrological state, overburden stress, and deformability properties, the onset of flowslides can indeed anticipate the initiation of slips throughout the duration of the infiltration process.

The above set of FS were calibrated by using data of unsaturated volcanic soils that were involved in a series of rainfall-induced flowslides (Greco et al., 2010). For instance, Fig. 3a and 3b shows the calibration of hydrologic functions by using Gardner's exponential functions for the WRC and HCF, respectively. A detailed description of the calibration procedures for the mechanical parameters can be found in Lizárraga and Buscarnera, 2017.

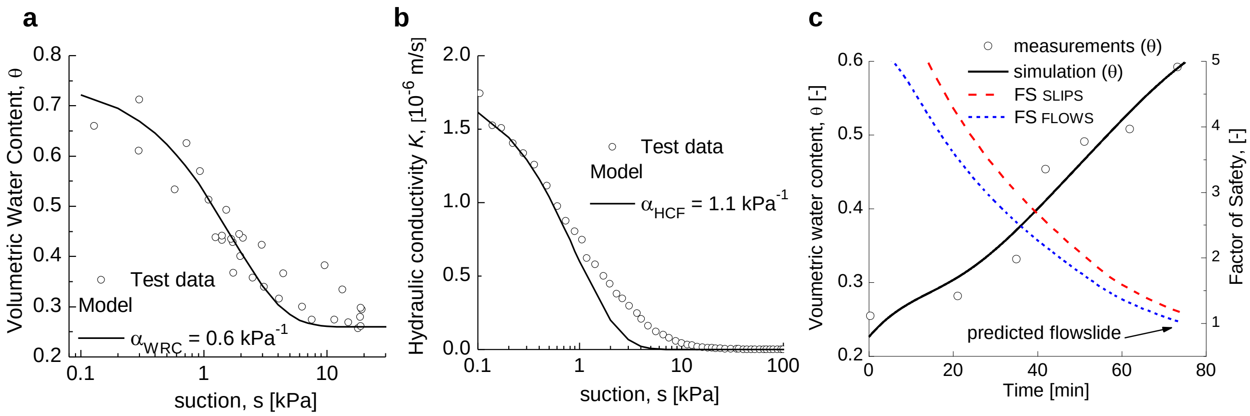

Fig. 3. Calibration of adopted hydrological models. (a) Water Retention Curve; (b) Hydraulic Conductivity Function; c) Results of numerical simulation. The model captures the variation of volumetric water content and the onset of a flowslide (FS_{FLOWS}<1) by the end of the test.

The performance of the calibrated FS was tested against results of highly-monitored flume tests that displayed different failure mechanisms upon infiltration. For instance, Fig. 3c shows a comparison between values of volumetric water content θ measured during a test (open circles) and FE simulation (thicker, black continuous line). Additionally, the evolution of both sets of FS are plotted. Note that values of FS_{FLOWS} are in close proximity to unity by the end of test (where a flowslide was detected). In other words, the calibrated model was able to satisfactorily reproduce the hydrologic behavior of slope and the onset of a flowslide event. It is worth noting that slips were observed to occur in other flume tests in which the same soil was used, but the material was deposited at different levels of porosity and initial degrees of saturation, thus highlighting the possible coexistence of such mechanisms under field conditions. Further details of the model performance can be found in Lizárraga and Buscarnera, 2017.

4. Regional analyses of landslide susceptibility

The solution of the coupled system of PDE has been implemented into a spatially-distributed modelling framework for regional landslide assessment. Specifically, the FE algorithm has been vectorized such that parallel simulations of coupled infiltration analyses can be performed simultaneously under a wide variety of model conditions. Such simulations are then linked to a Geographical Information System (GIS) platform to generate maps of landslide susceptibility over duration of a storm event. This allows the incorporation of different constitutive models, coupled-flow deformation analyses, layering, and distinct initial and boundary conditions, into a unified computational platform thus providing a versatile tool for regional landslide susceptibility. Details of the implementation procedures be found in Lizárraga and Buscarnera (2018).

The proposed methodology was applied to a series of landslides that occurred Campania (southern Italy). On May 4-5 of 1998, more than a hundred of shallow landslides occurred over an area of 60 km^2, after more than 40 hr of continuous rainfall. Most events were characterized as flowslides able to propagate downslope for several km, thus causing extensive damage and loss of life on the surrounding urban centers (Fig. 4). Detailed analyses of the meteorological aspects of the event, geological and geotechnical characteristics of the deposits and field monitoring studies have been widely documented elsewhere (Cascini et al., 2008; Crosta and Dal Negro, 2003; Guadagno et al., 2005).

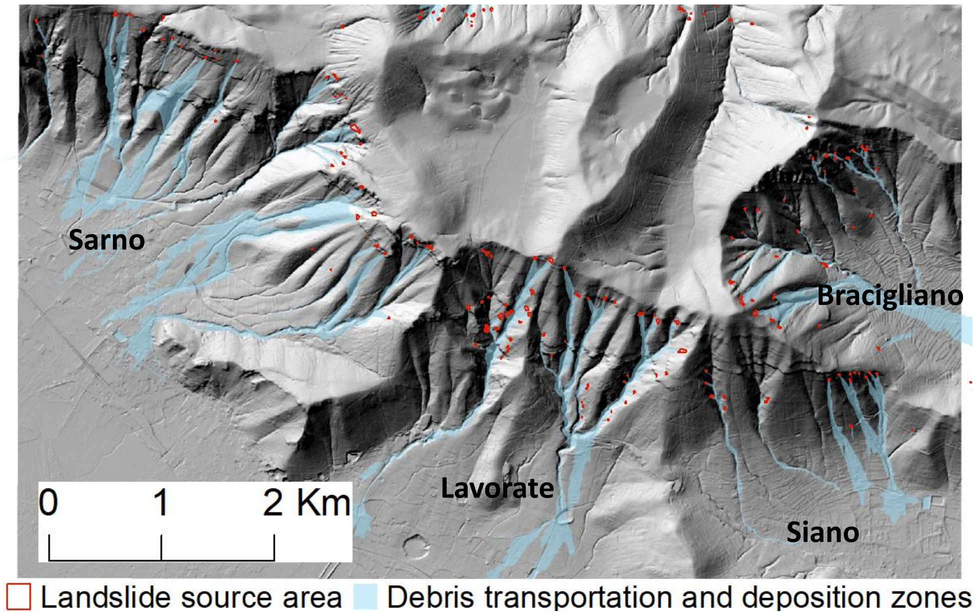

Fig. 4. Spatial distribution of shallow landslides in Campania (Southern Italy) after the rainfall events of 1998.

An example of model application for the municipality of Lavorate (south central sector of Fig. 4) is shown below. The spatial distribution of computed slips and flowslides by the end of the storm provides a reasonable agreement with the documented landslide source areas. Indeed, the ratio of successful prediction versus overpredicted areas is approximately 10, which is an improvement over previous studies performed in the same region (Sorbino et al., 2010). Additionally, approximate 70% of the predictions are classified as flowslides, which is in close agreement with the reported landslide inventory (Crosta and Dal Negro, 2003).

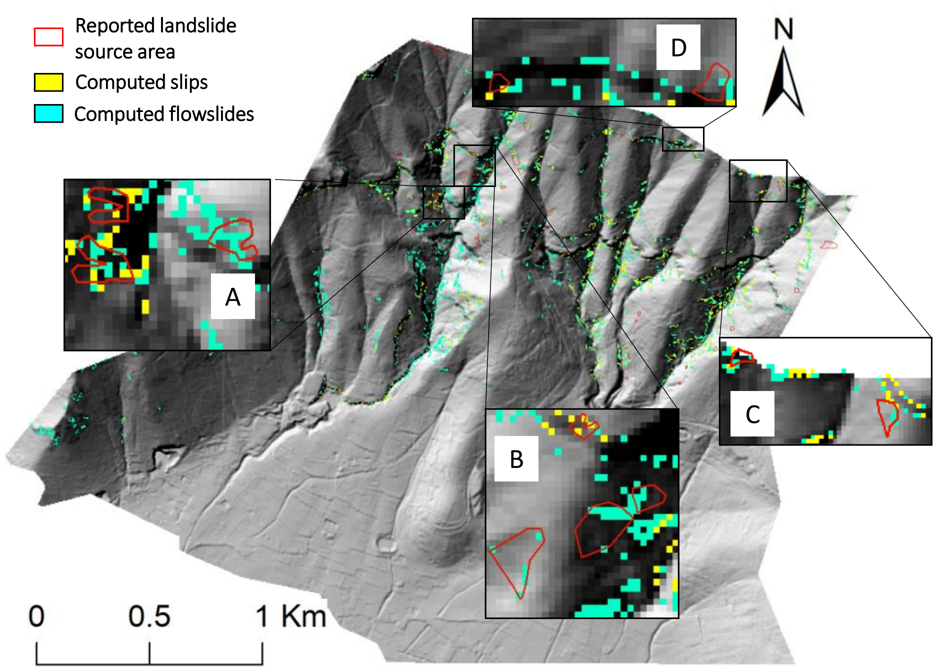

Fig. 5. Computed landslide susceptibility map for the municipality of Lavorate.

The temporal evolution of computed unstable area is shown in Fig 6. The upper continuous line reflects the cumulative fraction of computed unstable area accounting for both failure mechanisms, while the lower curve provides the partition between each failure mode. The first unstable slopes are computed at t = 24 hr and are classified as slips. After this, flowslides begin to appear around t = 30 hr. The performance of the computations improves over time, however, with the model predicting a marked increase in the rate of slope failures after t = 34 hr, i.e. much closer to the temporal interval of reported failures for this site.

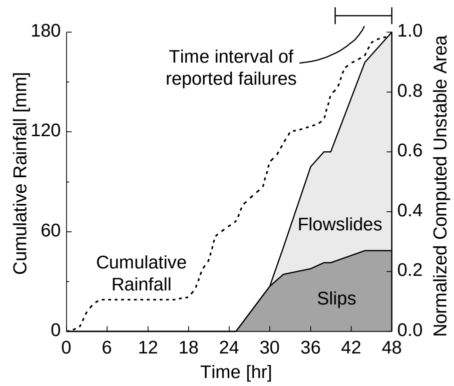

Fig. 6. Cumulated rainfall and temporal evolution of computed unstable area.

The above results were based on the assumption of vertical homogeneous slopes. Further improvements on model performance can be obtained by introduced the effect of layering. Examples of such application can be found in Lizárraga and Buscarnera, 2018.

5. Modelling spatial uncertainty in regional landslide hazard assesment

The model allows to incorporate the role of spatial uncertainty of input data on landslide susceptibility. Specifically, physical properties can be treated as spatially-correlated random fields (RF) with prescribed statistical attributes. In this manner, Monte Carlo simulations are performed for each realization and the results are aggregated and visualized in terms of maps of probability of landslide triggering that evolve over the duration of the storm. In the following, such approach is applied over a subsector located in the Siano municipality (south eastern corner of Fig. 4). Consider first Fig. 7 which shows three distinct realizations of RF of saturated hydraulic conductivity K_s, characterized by the same probability density function (*pdf*), but different levels of spatial correlation distance δ.

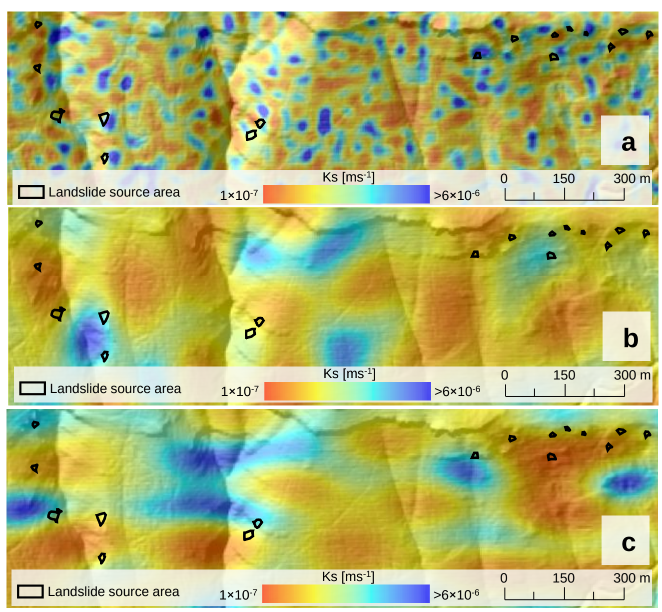

Fig. 7. Examples of random field realizations of *Ks* using a lognormal distribution (gaussian parameters mean = standard deviation = $1x10^{-6}$ ms^{-1}) (a) isotropic correlation distance δ = 10 m; (b) δ = 30 m; (c) anisotropic spatial correlation with δx = 60 m and δy = 30 m.

This parameter controls the variability of K_s as a function of proximity (Fenton and Griffiths, 2008). For instance, lower values of δ promotes the development highly-heterogeneous scenarios (Fig. 7a), and conversely, higher spatial correlation result in more homogeneous conditions (Fig. 8b). It is also possible to develop RF with anisotropic spatial correlation (Fig. 8c, δx>δy). In other words, in order to model the spatial uncertainty of a physical variable, one must specify not only its *pdf*, but also its degree of spatial variability.

The computed maps of probability of landslide triggering (p_f) using 100 Monte Carlo samples and a value of δx = δy = 30 m are shown in Fig. 8a and 8b for t =32 and 40 hr, respectively. For comparison, the reported landslide source areas were superposed (white hollow polygons). Note that as time progresses, areas with high levels of p_f (red zones) start to spread across the landscape. By t = 40 hr. most of the reported landslide source areas either coincide or are in the vicinity of cells with very high p_f, thus suggesting that the computations are in good agreement with the reported evidence.

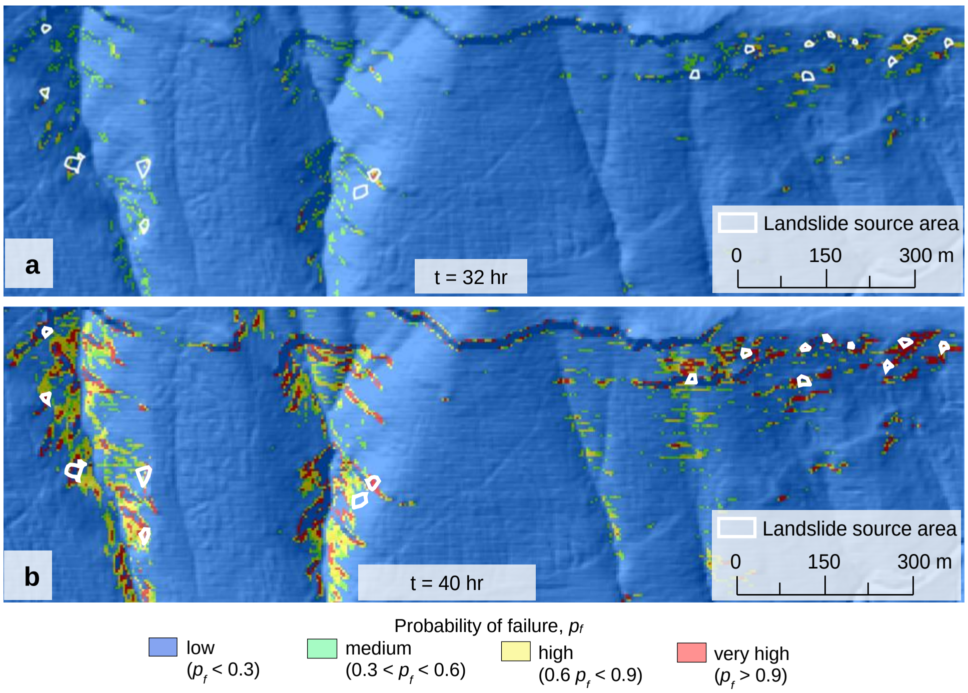

Fig. 8. Computed maps of probability of failure (a) t = 32 hr. and (b) t = 40 hr.

6. Conclusions

This contribution has described an integrated computational framework for regional assessment of rainfall-induced landslide triggering. The model relies on a vectorized numerical solver capable to perform multiple coupled flow-deformation analyses in unsaturated slopes under different conditions. The simulations are linked to a GIS platform to generate output maps of landslide susceptibility over the duration of a storm event.

Approaches to model flowslide triggering in terms of soil properties have been highlighted, and examples of application at both local and regional scales have been described. Additionally, a methodology to incorporate the role of spatial uncertainty of physical properties in the model simulations was presented, thus allowing the model outputs to be expressed in terms of probability of landslide triggering.

The proposed simulation platform fosters the use of laboratory data, georeferenced field measurements, and recent advances in stochastic and geomechanical modelling to construct an integrated virtual platform for regional landslide hazard assessment.

Acknowledgements

This work was supported by Grant No. CMMI-1324834 awarded by the US National Science Foundation

References

Baum, R.L., Godt, J.W. and Savage, W.Z., 2010, Estimating the timing and location of shallow rainfall-induced landslides using a model for transient, unsaturated infiltration: Journal of Geophysical Research: Earth Surface, 115, no. F3, doi:10.1029/2009JF001321.

Cascini, L., Cuomo, S. and Guida, D., 2008, Typical source areas of May 1998 flow-like mass movements in the Campania region, Southern Italy. Engineering Geology, 96(3-4), p. 107-125, doi:10.1016/j.enggeo.2007.10.003.

Crosta, G.B. and Dal Negro, P., 2003, Observations and modelling of soil slip-debris flow initiation processes in pyroclastic deposits: the Sarno 1998 event. Natural Hazards and Earth System Science, 3(1/2), p. 53-69, doi:10.5194/nhess-3-53-2003.

Dawson, R.F., Morgenstern, N.R. and Stokes, A.W., 1998, Liquefaction flowslides in Rocky Mountain coal mine waste dumps. Canadian Geotechnical Journal, 35(2), p. 328-343, doi:10.1139/t98-009.

Fenton G.A., and Griffiths, V.D., 2008, Risk assessment in geotechnical engineering. John Wiley & Sons, doi:10.1002/9780470284704.

Greco, R., Guida, A., Damiano, E. and Olivares, L., 2010, Soil water content and suction monitoring in model slopes for shallow flowslides early warning applications. Physics and Chemistry of the Earth, Parts A/B/C, 35(3-5), p. 127-136, doi:10.1016/j.pce.2009.12.003.

Guadagno, F.M., Forte, R., Revellino, P., Fiorillo, F. and Focareta, M., 2005, Some aspects of the initiation of debris avalanches in the Campania Region: the role of morphological slope discontinuities and the development of failure. Geomorphology, 66(1-4), p. 237-254, doi:10.1016/j.geomorph.2004.09.024.

Guzzetti, F., Carrara, A., Cardinali, M. and Reichenbach, P., 1999, Landslide hazard evaluation: a review of current techniques and their application in a multi-scale study, Central Italy. Geomorphology, 31(1), p.181-216, doi:10.1016/S0169-555X(99)00078-1.

Hungr, O., Evans, S.G. and Hutchinson, I., 2001, A Review of the Classification of Landslides of the Flow Type. Environmental & Engineering Geoscience, 7(3), p. 221-238, doi:10.2113/gseegeosci.7.3.221.

Iverson, R.M., 2014, Debris flows: behaviour and hazard assessment. Geology today, 30(1), p. 15-20, doi:10.1111/gto.12037.

Jefferies, M. and Been, K., 2015, Soil liquefaction: a critical state approach. CRC press, doi:10.4324/9780203301968.

Lizárraga, J.J. and Buscarnera, G., 2017, Safety factors to detect flowslides and slips in unsaturated shallow slopes. Géotechnique, 68(5), p. 442-450, doi:10.1680/jgeot.17.T.003.

Lizárraga, J.J. and Buscarnera, G., 2018, Spatially distributed modeling of rainfall-induced landslides in shallow layered slopes. Landslides, p. 1-11, doi:10.1007/s10346-018-1088-8.

Milledge, D.G., Bellugi, D., McKean, J.A., Densmore, A.L. and Dietrich, W.E., 2014, A multidimensional stability model for predicting shallow landslide size and shape across landscapes. Journal of Geophysical Research: Earth Surface, 119(11), p. 2481-2504, doi:10.1002/2014JF003135.

Montgomery, D.R. and Dietrich, W.E., 1994, A physically based model for the topographic control on shallow landsliding. Water resources research, 30(4), p. 1153-1171, doi:10.1029/93WR02979.

Picarelli, L., Olivares, L. and Avolio, B., 2008, Zoning for flowslide and debris flow in pyroclastic soils of Campania Region based on “infinite slope” analysis. Engineering Geology, 102(3-4), p. 132-141, doi:10.1016/j.enggeo.2008.03.015.

Sheng, D., Sloan, S.W., Gens, A. and Smith, D.W., 2003, Finite element formulation and algorithms for unsaturated soils. Part I: Theory. International journal for numerical and analytical methods in geomechanics, 27(9), p. 745-765, doi:10.1002/nag.295.

Sorbino, G., Sica, C. and Cascini, L., 2010, Susceptibility analysis of shallow landslides source areas using physically based models. Natural hazards, 53(2), p. 313-332, doi:10.1007/s11069-009-9431-y.

Wu, L.Z., Selvadurai, A.P.S., Zhang, L.M., Huang, R.Q. and Huang, J., 2016, Poro-mechanical coupling influences on potential for rainfall-induced shallow landslides in unsaturated soils. Advances in water resources, 98, p. 114-121, doi:10.1016/j.advwatres.2016.10.020.